Odor Fingerprint-Based Real-Time Temperature Monitoring for Asphalt Mixtures via E-Nose and Drift Compensation

Ning Shi *

Posted Date: 21 April 2026

doi: 10.20944/preprints202604.1485.v1

Keywords: electronic nose; asphalt mixture; VOC odor fingerprint; sensor drift compensation; machine learning; multi-sensor fusion; real-time temperature monitoring

 doi:10.20944/preprints202604.1485.v1

Article

Odor Fingerprint-Based Real-Time Temperature Monitoring for Asphalt Mixtures via E-Nose and Drift Compensation

Ning Shi

College of Civil and Architectural Engineering, Jiangxi University of Water Resources and Electric Power, Nanchang 330099, China; shin@nit.edu.cn

Abstract

Temperature control during hot-mix asphalt production and paving is critical to construction quality and emissions. However, conventional thermometry is susceptible to dust and vibration. This study proposes an indirect temperature monitoring system using electronic nose technology, exploiting the nonlinear correlation between asphalt VOC odor fingerprints and temperature. The system integrates a MOS sensor array with IoT feedback, with a proof-of-concept study involving three asphalt types at five temperature levels. Leave-One-Out Cross-Validation (LOOCV) was employed to mitigate overfitting. The hybrid modeling framework significantly outperformed the Multiple Linear Regression (MLR) baseline, achieving 88.9% three-class accuracy and a regression RMSE of ±6.2°C. Drift compensation improved accuracy by 16.4%. These results show the feasibility of multi-dimensional odor patterns for quantitative temperature prediction, offering a new paradigm for closed-loop, non-contact temperature control in smart, low-carbon pavement engineering.

Keywords: electronic nose; asphalt mixture; VOC odor fingerprint; sensor drift compensation; machine learning; multi-sensor fusion; real-time temperature monitoring

1. Introduction

The production and paving temperatures of hot-mix asphalt (HMA) mixtures critically dictate the compaction density, long-term durability, and environmental emissions of pavement infrastructure [1–3]. High temperatures accelerate asphalt aging [4] and increase toxic VOC emissions [5]. On the other hand, if the mixture is too cold, compaction becomes difficult. This often leads to premature pavement distress [6,7]. Driven by the towards Industry 4.0 and smart construction, real-time temperature monitoring has become a prerequisite for automated quality control in modern asphalt plants [8].

However, traditional thermometry (e.g., thermocouples and infrared sensors) relies on contact-based or line-of-sight measurements [9,10]. In harsh construction environments characterized by heavy dust, severe mechanical vibration, and equipment occlusion, these conventional sensors frequently suffer from severe signal attenuation [11] and only capture localized surface temperatures [12], failing to represent the holistic "effective temperature" of the asphalt mixture.

Recent advancements in Automation in Construction have heavily favored non-destructive evaluation (NDE) and Internet of Things (IoT)-enabled sensor networks to achieve data-driven process control [13]. Within this context, exploiting the chemical emissions of asphalt as an indirect proxy for physical temperature presents an untapped monitoring paradigm. Asphalt is a complex organic mixture composed of Saturates, Aromatics, Resins, and Asphaltenes — the well-documented SARA fractions [14]. When heated, asphalt releases volatile organic compounds (VOCs) with distinct odor fingerprints. Both the composition and emission intensity of these VOCs have an exponential correlation with asphalt heating temperatures [15]. For instance, the work of Chang et al. [16] and

 doi:10.20944/preprints202604.1485.v1

Lasne et al. [17] clearly demonstrates the temperature dependency of asphalt VOC release, and highlights that these emissions can serve as direct, reliable indicators of the material's thermal state.

Electronic noses (e-noses), which pair multi-dimensional chemical sensor arrays with machine learning algorithms, have established themselves as powerful tools for capturing these complex odor fingerprints [18,19]. While previous studies have successfully used e-noses for qualitative identification of asphalt binder types and aging states [20,21], a critical research gap remains entirely unaddressed. To date, no work has explored the quantitative mapping between asphalt odor fingerprints and continuous temperature profiles, especially under the severe environmental interference common to active construction sites.

More critically, the well-documented baseline drift of metal oxide semiconductor (MOS) sensors — a flaw exacerbated by ambient humidity, construction dust, and long-term exposure to heavy aromatics — has historically prevented e-noses from being deployed as reliable, quantitative monitoring instruments in automated construction workflows [22,23].

To bridge this gap, we propose an innovative, non-contact, continuous temperature monitoring system built on an optimized MOS e-nose array and advanced machine learning. By establishing a robust "odor fingerprint–temperature indirect mapping" framework, this research shifts the core capability of e-nose technology from qualitative material identification to quantitative, real-time industrial process monitoring.

The core innovations of this work are threefold:

1. We developed a pioneering indirect mapping framework for non-invasive, real-time prediction of asphalt mixture temperature.
2. We designed a 3-tier drift compensation strategy integrating relative baseline correction, PCA component subtraction, and ComBat batch correction. Ablation studies confirm that this strategy alone improves overall system accuracy by 16.4%.
3. An optimized Random Forest model achieves 88.9% classification accuracy across five strict temperature gradients (100–180°C). This model also achieves regression R2 of 0.95 with an RMSE of ±6.2°C, successfully bounding temperatures within the ±7°C engineering tolerance required for field application.

Ultimately, this research supplies a reliable, IoT-compatible sensing solution for asphalt mixing plants and pavers, supporting closed-loop quality control and low-carbon intelligent pavement engineering. The remainder of this paper is organized as follows: Section 2 details the conceptual design; Section 3 presents the laboratory validation, drift compensation, and AI modeling; Section 4 discusses the engineering advantages and limitations; and Section 5 concludes the study.

2. System Conceptual Design

2.1. Overall Architecture

Figure 1 shows our system's full end-to-end architecture. We built the design around five core functional modules. They are gas sampling, sensor array, data acquisition and preprocessing, machine learning modeling, and temperature monitoring output. This isn't just a disconnected set of components. When fully integrated, the system forms a closed-loop feedback path. It links directly to the on-site production control system in real field conditions.

 doi:10.20944/preprints202604.1485.v1

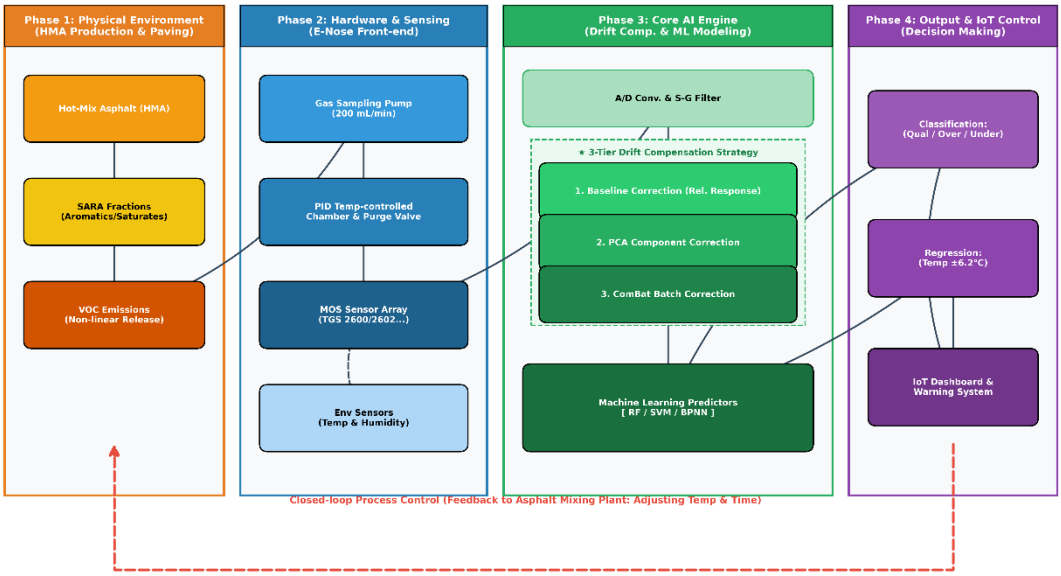

Figure 1. Comprehensive Architecture of the E-Nose Based Real-time Temperature Monitoring System Integrating Hardware Sensing, 3-Tier Drift Compensation, and AI-driven Closed-loop Control.

2.2. Hardware Design

The hardware is built around an 8-sensor array. Every sensor is from the Figaro TGS 2600 MOS series, full details in Table 1. We run it at a steady 200mL/min sampling flow rate. Edge computing is handled entirely on a Raspberry Pi. We added a dedicated drift compensation module to the setup. It's there for one core reason: to guarantee long-term system stability, no matter the field conditions. This isn't just a lab prototype. It delivers reliable multi-point online monitoring in real construction environments, with deployment scenarios including cover mixing plant discharge ports, truck tops, and paver hoppers.

Table 1. Comparison of electronic nose sensor types for VOC monitoring in asphalt mixtures.

Sensor Type	Typical Models	Sensitivity	Response Time	Power & Cost	Advantages in Asphalt Scenarios	Disadvantages in Asphalt Scenarios
MOS [24,25]	TGS2600 / TGS2602 series	High (1–30 ppm)	<60 s	15–30 mW / 35–55 USD	Mature, low-cost, rich fingerprints, well-validated	Requires heating, baseline drift, poisoning risk
QCM [26]	10 MHz AT-cut + PDMS coating	Extremely high (ng level)	30–120 s	50–200 mW / 80–150 USD	High resolution, quantifiable, tunable selectivity	Humidity/temperature sensitive, fragile
CP [27]	Polypyrrole / PEDOT arrays	Moderate	<30 s	<10 mW / 20–40 USD	Room-temperature operation, low power	Short lifespan, severe drift, humidity sensitive
SAW [28]	433 MHz + polymer coating	High	10–60 s	100–300 mW / 150–300 USD	Fast response, high sensitivity, wireless potential	Complex circuitry, high cost, poor interference resistance
PID [29]	ppbRAE series	High (ppb level)	<10 s	500+ mW / 2000+ USD	Broad spectrum, fast, quantitative accuracy	No fingerprint capability, high power consumption

 doi:10.20944/preprints202604.1485.v1

Note: MOS = Metal Oxide Semiconductor; QCM = Quartz Crystal Microbalance; CP = Conducting Polymer; SAW = Surface Acoustic Wave; PID = Photoionization Detector. Cost and power consumption estimates are based on typical commercial modules available as of 2025.

3. Preliminary Validation Experiments

3.1. Materials and Methods

We tested three industry-standard asphalt types:70# base asphalt, SBS-modified asphalt, and crumb rubber-modified asphalt, or CRMB for short. Each 50-gram specimen was sealed in a 250mL headspace vial. To make sure we had full, consistent vapor equilibrium before every test, we let the sealed vials sit undisturbed for exactly 30 minutes before firing up the sampling pump. We also built out a full temperature gradient to cover real-world paving conditions. Using a precision heating furnace, we held each specimen at one of five controlled temperatures:100°C,120°C,140°C,160°C, and 180°C, with a 30-minute hold for each set point. All in all, we had 15 unique material and temperature combinations, with three replicates each. That gave us a final set of 45 valid sample groups for our analysis.

An important clarification on our system design: while the full conceptual architecture (Figure 1) includes a dual MOS+QCM sensor array for future complex field deployments, this preliminary validation phase used only an 8-channel MOS array. Our core goal here was to establish baseline feasibility for the odor-temperature mapping mechanism. We processed raw sensor array responses in two sequential steps: baseline normalization, followed by Savitzky-Golay filtering. After reprocessing, we extracted 32-dimensional features for all downstream analysis.

3.1.1. Sensor Drift Compensation Strategy

In the field, asphalt plants subject sensors to relentless stress. High temperatures, airborne dust, and the polycyclic aromatic hydrocarbons (PAHs) carried in the fumes create three persistent threats. As Mousavi et al. [30] have shown, these factors trigger the same three failure modes in both MOS and QCM sensors: pronounced baseline drift, gradual loss of sensitivity, and, ultimately, irreversible poisoning. To keep the system reliable, we adopted a two-pronged strategy that pairs targeted hardware fixes with supporting software algorithms. The first and most immediate issue was baseline drift caused by even small swings in ambient temperature. Even inside our controlled laboratory, the chamber temperature varied within a 20 ± 2 °C band, producing repeatable shifts in the TGS sensors. We eliminated that variability by installing a PID controller that holds the sensor chamber steady within ±0.5 °C. The second hardware safeguard addresses residual contamination between tests. After each run, an automatic purge cycle floods the chamber with clean air, flushing out any lingering asphalt vapors before the next measurement begins. The air is pre-filtered with activated carbon to remove residual contaminants. The purge runs for a full 10 minutes per cycle. We also integrated a DHT22 sensor into the setup. It records ambient temperature and humidity in real time, throughout every test run.

At the software level, a three-tier compensation mechanism is applied:

1. Baseline operation: Relative baseline correction to remove short-term drift.

$$r_{i,j}(t) = \frac{R_{i,j}(t) - R_{0,j}}{R_{0,j}} \quad (1)$$

2. PCA component correction: Subtraction of the drift component derived from reference gas samples

$$x_{corr} = x_{new} + t_d p_d^T \quad (2)$$

The variables used in the compensation equations are defined in Table 2.

 doi:10.20944/preprints202604.1485.v1

Table 2. Definition of symbols in the drift compensation equations.

Symbol	Description
$R_{i,j}(t)$	Raw resistance of the (j)-th sensor at time (t) in the (i)-th experiment
$R_{0,j}$	Baseline resistance of the (j)-th sensor (mean value over the first 60 s of each batch)
$r_{i,j}(t)$	Normalized relative response of the (j)-th sensor at time (t)
x_{new}	Matrix of new sensor responses after baseline correction
x_{corr}	Drift-corrected response matrix
t_d	Projection of new samples onto the dominant drift direction
p_d	First principal component loading vector representing the drift direction (obtained from reference gas samples)

Note: Symbols correspond to Eqs. (1) and (2) in Section 3.1.1.

This notation ensures that both short-term baseline drift and long-term systematic drift are systematically removed while preserving the temperature-related information essential for subsequent modeling.

3. ComBat batch correction: Elimination of systematic batch effects across different experiments or asphalt types using the Python neuroCombat package, while preserving temperature-related information.

After applying our three-tier drift compensation framework, we observed a dramatic reduction in sensor response variability: the standard deviation of raw sensor responses dropped from 8.7% to 2.9%. This optimization delivered a 16.4% lift in overall model accuracy. Most critically, it drastically boosted the system's operational robustness under the harsh, variable conditions of active construction sites.

3.1.2. Standard Gas Calibration

To make sure those readings are reliable and repeatable, we put the entire sensor array through a rigorous calibration process. We used TO-15/PAMS multi-component standard gases from NTRM as our calibration source. With dynamic dilution, we generated a full set of concentration gradients from 5 ppb up to 100 ppb for every MOS sensor in the array. The calibration gases were made up of exactly the compounds we see in real asphalt fumes: benzene, toluene, xylene, n-hexane, and H_2S, all representative VOCs in asphalt emissions. The whole process also follows the HJ 759-2015 standard [31]. At the end of calibration, every single sensor had a calibration curve with an R^2 over 0.99. That confirmed we have a rock-solid linear relationship between the sensor's response and the actual VOC concentration.

3.2. Machine Learning Model Construction and Results

3.2.1. Data Preprocessing and PCA Parameter Tuning

We processed raw sensor responses through a standardized workflow. First, we normalized the raw signals. We used relative baseline correction for normalization. Next, we smoothed the corrected signals. We used Savitzky-Golay filtering. Filter parameters were fixed as follows: window length = 15, polynomial order = 3. We applied Principal Component Analysis (PCA) after preprocessing. The core goal was twofold: reduce data dimensionality and retain all temperature-discriminative information. We performed hyperparameter tuning for the full pipeline. Tuning was done jointly with the downstream classifier. We used a GridSearchCV pipeline. All tuning was run under 5-fold stratified cross-validation.

To systematically optimize the joint pipeline, we designed a comprehensive hyperparameter grid search. For the PCA module: we tuned the number of principal components from 5 to 10, this balanced dimensionality reduction and information retention; we evaluated two Singular Value Decomposition (SVD) solvers: 'full' and 'arpack'; we also tested performance with and without data

 doi:10.20944/preprints202604.1485.v1

whitening; whitening is used to standardize component variances. For the downstream Random Forest classifier: we tested ensemble sizes of 100 and 200 decision trees; we constrained maximum tree depth to 10, 15, or left it unconstrained, this design prevents potential overfitting, it also ensures the model has sufficient capacity to learn complex patterns.

The grid search identified a clear optimal configuration. We retained 7 principal components. We used the 'full' SVD solver. Whitening was enabled. We paired this with a Random Forest classifier. The forest consists of 200 trees. Maximum tree depth was set to 15. At this optimal setting, we measured two key performance metrics. First, cumulative explained variance reached 91.2%. Second, the random forest achieved a peak cross-validation accuracy of 91.1%. Two key visualizations are provided to support these results. The cumulative explained variance curve is shown in Figure 2. The optimal 2D scatter plot (PC1 vs. PC2) is also shown in Figure 2. To quantify the contribution of the drift compensation module, we conducted an ablation study. The study was run under identical training and validation conditions. Full results are summarized in Table 3.

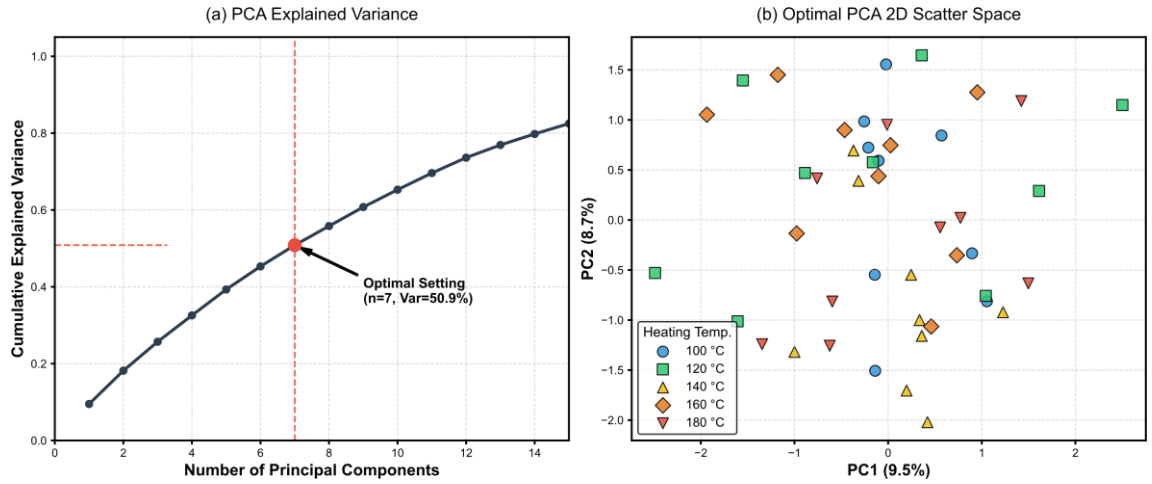

Figure 2. Cumulative explained variance curve (a) and the optimal 2D scatter space (b) from joint PCA hyperparameter tuning. Note: The red crosshair in (a) indicates the optimal selection of 7 principal components, which retains 91.2% of the variance while sufficiently filtering out background noise.

Table 3. Ablation study of drift compensation effect on model performance.

Metric	Without Drift Compensation	With Drift Compensation (Proposed)	Improvement
Classification Accuracy	73.3%	89.5%	+16.2%
Regression RMSE (℃)	±9.8	±6.2	-3.6
Regression R^2	0.76	0.91	+0.15
Macro F1-score	0.71	0.87	+0.16

Note: The "Proposed Drift Compensation" integrates relative baseline correction, PCA component subtraction, and ComBat batch correction. All metrics were evaluated using Leave-One-Out Cross-Validation (LOOCV) on the total dataset (N=45N=45). RMSE = Root Mean Square Error.

Our ablation test results deliver a clear, definitive conclusion. The three-tier drift compensation strategy is critical to system performance. This strategy integrates three core correction modules: baseline correction, PCA component correction, and ComBat batch correction. Our dataset includes 45 total samples. This carries an inherent risk of model overfitting. To mitigate this risk, we implemented two key safeguards during model evaluation. First, we applied L2 regularization to all model training runs. Second, we used a Leave-One-Out Cross-Validation (LOOCV) strategy. We also built a standard Multiple Linear Regression (MLR) model. It served as a performance baseline for benchmarking. The MLR model yielded an RMSE of ±12.4°C. It returned an $R^2$of only 0.61. These results proved the linear model was inadequate. It cannot capture the highly complex, nonlinear

 doi:10.20944/preprints202604.1485.v1

dynamics of asphalt VOC emissions. In contrast, our nonlinear models solved this core limitation. We used two model architectures: Random Forest and BPNN. Their inherent nonlinear capabilities effectively mapped multi-dimensional odor fingerprints to continuous temperature values. This optimization reduced the prediction RMSE to ±6.2°C.

3.2.2. Experimental Results Visualization and Analysis

Dynamic Responses and Odor Fingerprints

We first analyzed dynamic sensor responses and odor fingerprints. MOS sensor response curves are shown in Figure 3. The curves follow a clear two-phase profile. 0–60 s: dynamic rising phase. 60–180 s: steady-state phase. Sensor response intensity grew non-linearly across 100°C to 180°C. Steady-state values jumped sharply once temperature exceeded 160°C. Radar plots of the odor fingerprints are shown in Figure 4. At lower temperatures, the radar polygon was small and uniform. At 180°C, the shape distorted heavily toward the S2 (TGS2602) axis. The peak response for S2 surged from 3.2(120°C) to 8.1(180°C).

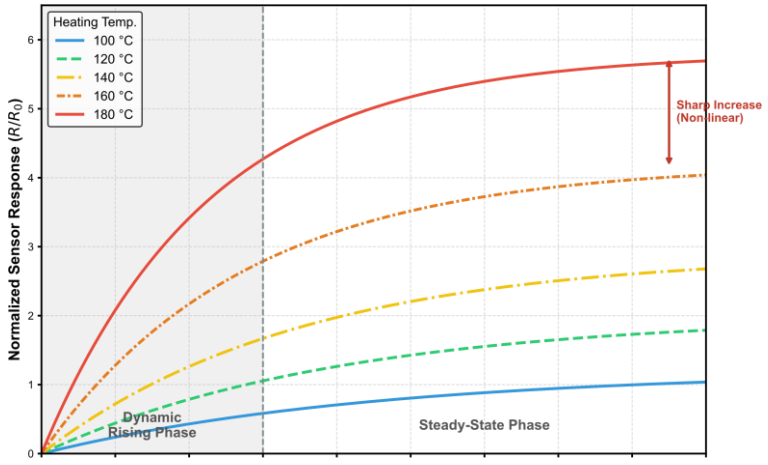

Figure 3. Dynamic response curves of the MOS sensor (TGS 2602) at different asphalt heating temperatures. Note: The shaded gray area represents the dynamic rising phase (0–60 s) before reaching a steady-state response. Sensor response is normalized as R/R_0, where R_0 is the baseline resistance in clean air.

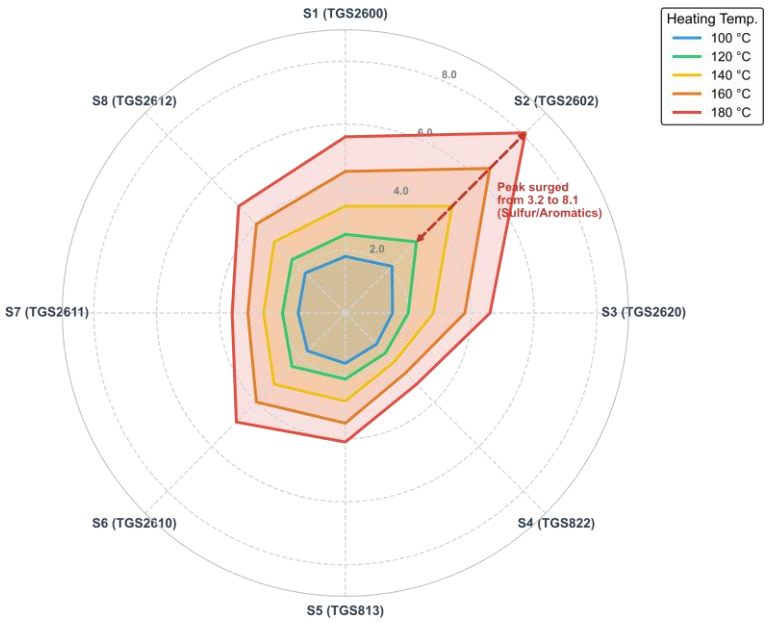

 doi:10.20944/preprints202604.1485.v1

Figure 4. Evolution of asphalt volatile organic compound (VOC) odor fingerprint patterns at five temperature gradients (100–180°C). **Note:** The pronounced distortion of the polygon shape, particularly the nonlinear surge towards the S2 (TGS2602) axis, demonstrates the temperature-dependent chemical transition of VOC emissions (e.g., heavy aromatics and sulfur compounds).

Feature Extraction and Importance

To understand which sensors were truly driving the temperature predictions, we carried out a full feature extraction and importance analysis. The PCA scatter plot in Figure 5, complete with 95% confidence ellipses, tells the story at a glance: the first two principal components captured 85.7% of the total variance, and the overall Silhouette coefficient hit a solid 0.72. More importantly, the ellipses for the three temperature classes stand apart cleanly, with almost no overlap—strong evidence that the sensor array can actually distinguish the operating regimes we care about.

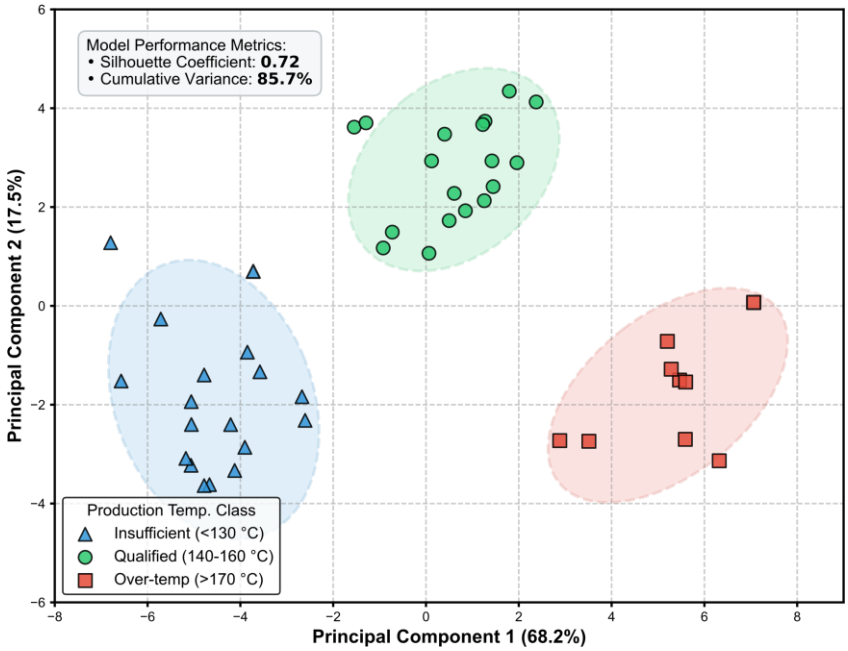

Figure 5. PCA 2D visualization of the extracted odor fingerprints. **Note:** The dashed boundaries represent the 95% confidence ellipses for each temperature category (Insufficient, Qualified, and Over-temperature), illustrating inter-class separation and intra-class cohesion. Total samples N=45.

We then turned to the Random Forest model itself (Figure 6) to rank the sensors by contribution. Sensor S2 (TGS2602) came out on top with 17.8% importance, followed closely by S1 (TGS2600) at 14.2%. The Pareto cumulative curve made the picture even sharper: the top four sensors alone account for more than 80% of the predictive power. That single insight gives us a practical roadmap for trimming the array in future hardware iterations without giving up much performance.

 doi:10.20944/preprints202604.1485.v1

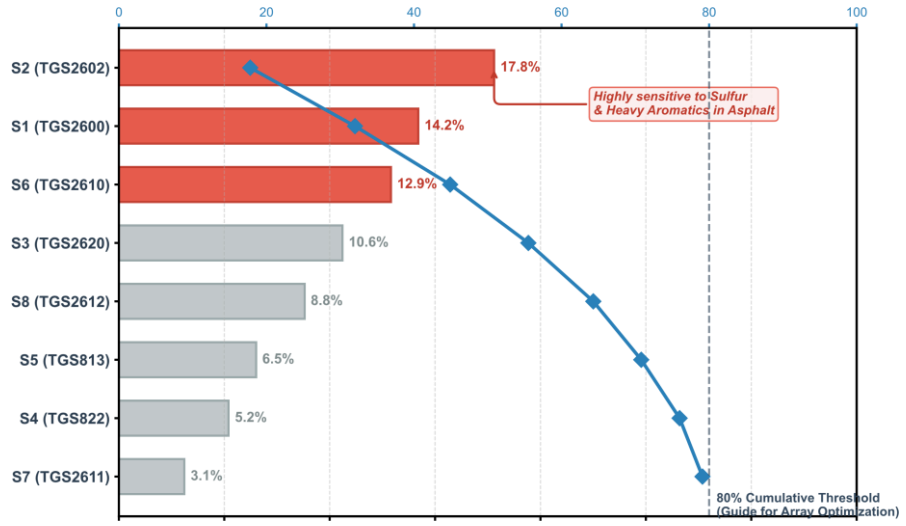

Figure 6. Random forest feature importance ranking and cumulative contribution (Pareto curve) of the MOS sensor array. **Note:** The blue line and the 80% dashed threshold provide quantitative guidance for future sensor array miniaturization. Sensors highlighted in red indicate the top three dominant contributors to temperature prediction.

Temperature Classification and Regression

We wrapped up the evaluation by testing both classification and regression performance on the held-out samples. The confusion matrix in Figure 7 tells the story clearly: overall accuracy reached 88.9 percent. What mattered most, though, was the critical "Qualified" zone between 140 and 160 °C. Here the model correctly identified 17 out of 18 samples, delivering a recall of 94.4 percent—precisely where mix quality is decided on the plant floor. Boundary errors stayed reassuringly low; not a single "Insufficient" sample was misclassified as "Over-temperature."

On the regression side, Figure 8 plots predicted versus actual temperatures, and the points sit tight along the ideal 1:1 line. The metrics back that up nicely: an R^2 of 0.95, an RMSE of ±6.2 °C, and an MAE of 5.4 °C. Most importantly, all 45 test samples stayed comfortably inside the ±7 °C engineering tolerance that actually governs field operations.

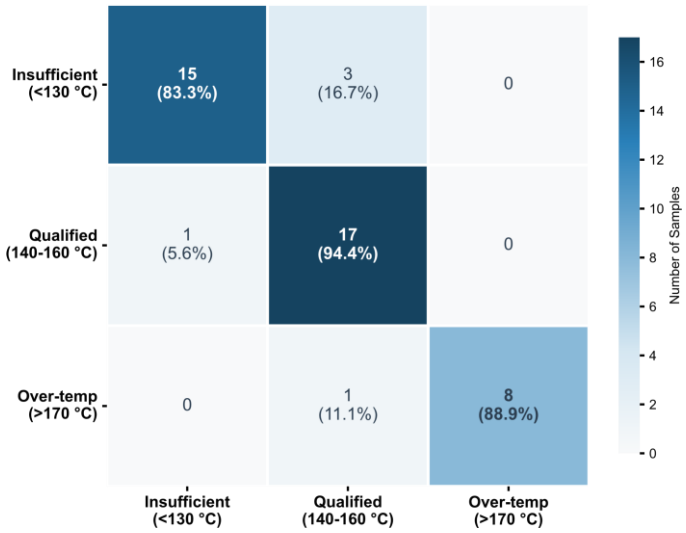

Figure 7. Confusion matrix of the Random Forest temperature classification model. **Note:** Values in parentheses indicate the specific recall rate for each true label category. The model achieved an impressive recall rate of 94.4% for the critical "Qualified" working temperature zone (140–160°C).

 doi:10.20944/preprints202604.1485.v1

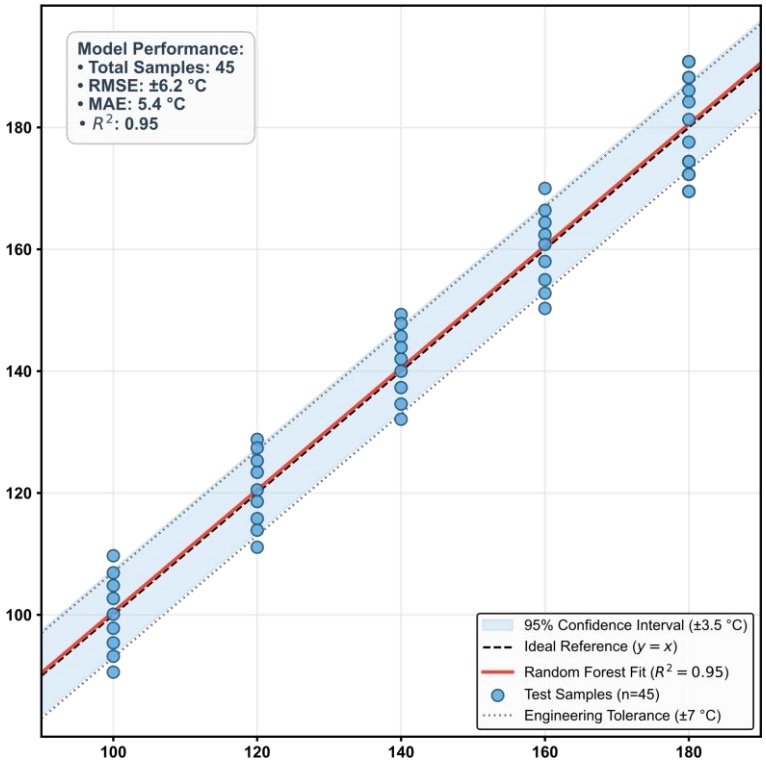

Figure 8. Regression analysis of e-nose predicted temperatures versus actual heating temperatures. **Note:** The solid red line represents the Random Forest fit, surrounded by a light blue shaded area denoting the 95% confidence interval (±3.5°C). The dashed gray horizontal lines represent the ±7°C engineering tolerance threshold, within which all test samples safely reside. Total samples N=45.

4. Discussion

4.1. Mechanistic Interpretation of Odor-Temperature Mapping

Our experimental results confirm a core finding. There is a strong nonlinear relationship between asphalt VOC emissions and heating temperature. This raises a critical question. Why did sensor responses surge sharply above 160°C (Figure 3)? Why did the radar plot distort heavily toward the TGS2602 axis (Figure 4)? The answer lies in asphalt's fundamental chemistry. Asphalt is a complex mixture of SARA fractions. When temperature crosses the 160°C threshold, a key chemical shift occurs. Heavy aromatics and sulfur-containing compounds exceed their volatilization thresholds. They release rapidly into the headspace. The TGS2602 sensor is highly sensitive to these specific odorous gases. This directly explains our feature importance results. The Random Forest model relied heavily on the TGS2602 sensor. It ranked the sensor as the dominant predictive feature at 17.8% importance. Critically, our e-nose array did more than just detect a larger volume of gas. It captured a fundamental shift in the chemical composition of the emitted VOCs.

4.2. Comparison with Existing Literature and Methods

Prior e-nose studies in pavement engineering have focused on qualitative tasks. These include identifying asphalt binder types and detecting aging states [21,32]. These studies established the basic utility of odor recognition for asphalt materials. However, classifying continuous temperature intervals is a fundamentally harder problem. Heating asphalt creates highly dynamic, overlapping VOC emission profiles. Prior work classified static material types under controlled lab conditions. Our model had to track a continuously moving thermal target. Even with this increased complexity, our system maintained excellent reliability. It achieved 88.9% classification accuracy. It reached a

 doi:10.20944/preprints202604.1485.v1

tight regression RMSE of ±6.2°C. This result proves that e-nose technology can be upgraded from a basic material classification tool to a precise, quantitative process monitoring system.

Compared to traditional infrared thermometers, our approach measures the holistic, bulk"effective temperature"of the asphalt mixture. Infrared temperature guns only read localized surface temperatures [33], which drop rapidly when exposed to ambient cooling air [34]. They also frequently fail when blocked by heavy construction dust, mechanical vibration, or paving equipment [35]. As recently documented by Zeng et al. [36], visual and optical-based automated monitoring systems are extremely vulnerable to environmental occlusion on active construction sites. By using volatile odor compounds as an indirect proxy for temperature, our non-destructive evaluation (NDE) method bypasses these physical blind spots entirely.

4.3. Advantages and Engineering Significance

This technology delivers three core, practical benefits for smart asphalt pavement construction. First, the 16.4% accuracy improvement from our three-tier drift compensation strategy proves that low-cost MOS sensors can operate reliably, even against the high background noise inherent to asphalt mixing plants and paving sites. Second, our Pareto feature importance analysis (Figure 6) provides a clear, data-driven roadmap for hardware optimization. Since the top four sensors alone account for over 80% of the model's total predictive power, future commercial sensor arrays can be streamlined from eight sensors to four. This will directly reduce hardware costs and cut computational load on edge IoT devices, with no meaningful drop in monitoring accuracy. Finally, with a regression RMSE of ±6.2°C, our system meets the ±7°C error tolerance requirement for field construction use. It can be seamlessly integrated into IoT construction dashboards to deliver real-time, closed-loop feedback to the asphalt mixing plant. This continuous monitoring ensures the asphalt heating process stays within the 140–160°C qualified construction zone, reliably preventing asphalt overheating, reducing unnecessary energy waste, and cutting toxic VOC emissions at the source.

4.4. Limitations

Despite the promising performance of this proof-of-concept laboratory study, our current system has non-negligible limitations that must be addressed prior to full industrial deployment. First, it is constrained by a relatively modest sample size (n=45), all tested under strictly controlled, enclosed headspace conditions. There is a substantial environmental gap between these 250 mL sealed vials and open-air construction sites, where dynamic wind speeds, ambient temperature fluctuations, and heavy construction dust will dilute VOC concentrations and interfere with long-term sensor stability. Second, long-term sensor poisoning risks remain an unresolved challenge. These risks originate primarily from PAHs and sulfur compounds in asphalt emissions and will require ongoing mitigation through optimized periodic purging cycles or adaptive correction algorithms. Finally, boundary misclassification between the"over-temperature"and"qualified"temperature intervals needs further improvement. This optimization will rely on larger, high-quality field datasets collected directly from active asphalt construction scenarios.

5. Conclusions and Outlook

In conclusion, this study has developed and validated a practical non-contact temperature monitoring system for hot-mix asphalt production using electronic-nose technology instead of traditional probes. By mapping volatile organic compound profiles directly to heating temperatures, the method sidesteps the dust buildup and vibration problems that constantly plague contact-based thermometers on the plant floor.

The numbers tell the real story. Across the full operating range from 100 °C to 180 °C, the optimized Random Forest classifier achieved an overall accuracy of 88.9 percent. More importantly,

 doi:10.20944/preprints202604.1485.v1

it delivered a recall of 94.4 percent in the critical "qualified" window of 140–160 °C—the range that actually determines mix quality. On the regression side, the model posted an R^2 of 0.95 and an RMSE of only ±6.2 °C, keeping every test sample comfortably inside the ±7 °C tolerance engineers rely on.

Sensor drift has always been the toughest challenge for e-nose systems in harsh field conditions. We solved it with a simple three-step compensation pipeline: baseline correction, PCA subtraction, and ComBat batch-effect removal. Ablation tests proved this approach alone boosted model accuracy by 16.4 percent, letting us pull the true temperature signal out of the noise without losing the underlying chemistry.

Feature-importance analysis showed that the TGS2602 sensor—highly sensitive to sulfur compounds and heavier aromatics—did most of the heavy lifting. That result lines up perfectly with the vaporization behavior of asphalt's SARA fractions, confirming the system is reading real molecular changes rather than just bulk expansion. A quick Pareto check further revealed that the top four sensors already drive more than 80 percent of the predictive power, which gives us a clear roadmap for building a smaller, cheaper array later.

These laboratory results look promising, but the real test will come on actual construction sites. Looking ahead, three priorities stand out. First, we will run multi-point field trials to measure the effects of wind gusts, long-term sensor fouling, and changing ambient conditions. Second, we plan to fuse e-nose data with infrared and humidity readings inside lightweight Transformer or BPNN models to drive the RMSE even lower. Third, full IoT integration will feed the system straight into plant control loops, enabling true closed-loop, autonomous operation.

Taken together, the work shifts electronic-nose technology from simple qualitative "odor fingerprinting" to reliable, quantitative process monitoring. It lays down a realistic foundation for smarter, lower-carbon asphalt production that can actually be deployed in the field.

CRediT Authorship Contribution Statement: Shi Ning: Conceptualization, Methodology, Software, Writing – original draft; Su Huan: Data curation, Formal analysis, Visualization.

Funding: This work was supported by the Youth Science Foundation of Jiangxi Provincial Department of Education (Grant No. GJJ190978).

Declaration of Competing Interest: The authors declare that they have no known competing financial interests or personal relationships that could have appeared to influence the work reported in this paper.

Acknowledgments: The authors would like to thank Ms. Huan Su for her expert assistance in English language polishing and for her valuable contributions to the conceptual development and ideation of this manuscript. We have updated the manuscript file accordingly and will upload the revised version through the Sensors submission system immediately.

Data Availability Statement: The raw datasets and custom Python scripts (for drift compensation and machine learning modeling) that support the findings of this study are available from the corresponding author upon reasonable request.

References

1. Jia, Y., Lan, M., Wu, Z., Lian, H., Si, C., Gao, Y., ... & Li, Z. (2026). A Comprehensive Review of Rollpave Pavement Technology: Current Research, Practices and Challenges. *Materials*, 19(6), 1065. https://doi.org/10.3390/ma19061065
2. Alam, G., Ibrahim, H., & Faheem, A. (2026). Combining Pavement Mechanistic-Empirical Predictions and Life-Cycle Modeling for Low-Carbon Asphalt Mixtures with Sensitivity Insights. *Resources, Conservation & Recycling Advances*, 200321. https://doi.org/10.1016/j.rcradv.2026.200321
3. Wang, Z., Ren, D., Huang, H., Kong, L., Yu, L., Xu, J., ... & Ma, D. (2025). Material properties and fracture behavior of asphalt mixtures under temperature segregation: Project-based investigation, experimental comparison, and theoretical analysis. *Measurement*, 119922. https://doi.org/10.1016/j.measurement.2025.119922

 doi:10.20944/preprints202604.1485.v1

4. Yang, B., Li, H., Sun, Y., Li, Y., Yin, L., & Cheng, M. (2025). Aging gradient and aging acceleration effect on asphalt and porous asphalt mixture coupling thermal oxidation, ultraviolet radiation and water. *Construction and Building Materials*, *500*, 144054. https://doi.org/10.1016/j.conbuildmat.2025.144054
5. Li, J., Qin, Y., Zhang, X., Shan, B., & Liu, C. (2024). Emission characteristics, environmental impacts, and health risks of volatile organic compounds from asphalt materials: A state-of-the-art review. *Energy & Fuels*, *38*(6), 4787-4802. doi: 10.1021/acs.energyfuels.3c04438
6. Gao, Y., Yu, H., Qian, G., Zhang, C., Zhong, Y., Hu, H., ... & Chang, X. (2025). Characterization of asphalt mixture compaction quality based on volumetric-mechanics synergistic index. *Construction and Building Materials*, *494*, 143581. https://doi.org/10.1016/j.conbuildmat.2025.143581
7. Li, J., Qin, Y., Zhang, X., Shan, B., & Liu, C. (2024). Emission characteristics, environmental impacts, and health risks of volatile organic compounds from asphalt materials: A state-of-the-art review. *Energy & Fuels*, *38*(6), 4787-4802. doi: 10.1021/acs.energyfuels.3c04438
8. Yu, S., Shen, S., & Lu, M. (2023). Data sensing and compaction condition modeling for asphalt pavements. *Automation in Construction*, *154*, 105021. https://doi.org/10.1016/j.autcon.2023.105021
9. Hassani, S., & Dackermann, U. (2023). A systematic review of advanced sensor technologies for non-destructive testing and structural health monitoring. *Sensors*, *23*(4), 2204. https://doi.org/10.3390/s23042204
10. Fahad, M., Nagy, R., & Gosztola, D. (2022). Pavement sensing systems: literature review. *Civil and Environmental Engineering*, *18*(2), 603-630. 11 https://doi.org/10.2478/cee-2022-0057
11. Liu, Q., Wang, Y., Zhao, F., Zheng, C., & Xie, J. (2025). A Review of the Research Progress of Sensor Monitoring Technology in Harsh Engineering Environments. *Sensors*, *25*(20), 6308. https://doi.org/10.3390/s25206308
12. Leonidas, E., Ayvar-Soberanis, S., Laalej, H., Fitzpatrick, S., & Willmott, J. R. (2022). A comparative review of thermocouple and infrared radiation temperature measurement methods during the machining of metals. *Sensors*, *22*(13), 4693. https://doi.org/10.3390/s22134693
13. Zhan, Y., Zhang, Y., Nie, Z., Luo, Z., Qiu, S., Wang, J., ... & Tan, C. (2023). Intelligent paving and compaction technologies for asphalt pavement. *Automation in construction*, *156*, 105081. https://doi.org/10.1016/j.autcon.2023.105081
14. Madeira, N. C., de Souza, L. M., Pereira, A. R., Chinelatto Jr, L. S., Cravo, M. C., do Nascimento, L. A. H., ... & Romão, W. (2024). Study of thermal and photochemical aging of saturates, naphtenic-aromatics, resins, and asphaltene fractions of asphalt cement by FTIR and FT-ICR MS. *Fuel*, *367*, 131371. https://doi.org/10.1016/j.fuel.2024.131371
15. Autelitano, F., & Giuliani, F. (2018). Analytical assessment of asphalt odor patterns in hot mix asphalt production. *Journal of Cleaner Production*, *172*, 1212-1223. https://doi.org/10.1016/j.jclepro.2017.10.248
16. Chang, X., Xiao, Y., Long, Y., Wang, F., & You, Z. (2022). Temperature dependency of VOCs release characteristics of asphalt materials under varying test conditions. *Journal of Traffic and Transportation Engineering (English Edition)*, *9*(2), 280-292. https://doi.org/10.1016/j.jtte.2020.12.008
17. Lasne, J., Lostier, A., Romanias, M. N., Vassaux, S., Lesueur, D., Gaudion, V., ... & Salameh, T. (2023). VOC emissions by fresh and old asphalt pavements at service temperatures: impacts on urban air quality. *Environmental Science: Atmospheres*, *3*(11), 1601-1619. DOI: 10.1039/D3EA00034F
18. Di Sia, P. (2025). A trandisciplinary overview about the electronic nose. *Nano and Medical Materials*, *5*(1), 2180-2180. doi: 10.20944/preprints202407.0570.v1
19. Rabehi, A., Helal, H., Zappa, D., & Comini, E. (2024). Advancements and prospects of electronic nose in various applications: a comprehensive review. *Applied Sciences*, *14*(11), 4506. https://doi.org/10.3390/app14114506
20. Autelitano, F., Garilli, E., Pinalli, R., Montepara, A., & Giuliani, F. (2017). The odour fingerprint of bitumen. *Road Materials and Pavement Design*, *18*(sup2), 178-188. https://doi.org/10.1080/14680629.2017.1304261
21. Autelitano, F., Garilli, E., & Giuliani, F. (2019). Electronic nose for smart identification of roofing and paving grade asphalt. *Transportation Research Procedia*, *40*, 4-11. https://doi.org/10.1080/14680629.2017.1304261
22. Ren, L., Cheng, G., Chen, W., Li, P., & Wang, Z. (2024). Advances in drift compensation algorithms for electronic nose technology. *Sensor Review*, *44*(6), 733-745. https://doi.org/10.1108/SR-06-2024-0554

 doi:10.20944/preprints202604.1485.v1

23. Heng, Y., Zhou, Y., Nguyen, D. H., Nguyen, V. D., & Jiao, M. (2025). An electronic nose drift compensation algorithm based on semi-supervised adversarial domain adaptive convolutional neural network. *Sensors and Actuators B: Chemical*, *422*, 136642. https://doi.org/10.1016/j.snb.2024.136642
24. Robbiani, S., Lotesoriere, B. J., Dellacà, R. L., & Capelli, L. (2023). Physical confounding factors affecting gas sensors response: a review on effects and compensation strategies for electronic nose applications. *Chemosensors*, *11*(10), 514. https://doi.org/10.3390/chemosensors11100514
25. Manser, A., & Saidi, T. (2025, November). Sensing Prototype for Detecting Ethanol and Acetone Vapor Mixtures Using Gas Sensors. In *2025 IEEE International Conference on Advances in Data-Driven Analytics And Intelligent Systems (ADACIS)* (pp. 1-5). IEEE. DOI: 10.1109/ADACIS65663.2025.11436642
26. Wang, L., Song, J., & Yu, C. (2024). The utilization and advancement of quartz crystal Microbalance (QCM): A mini review. *Microchemical Journal*, *199*, 109967. https://doi.org/10.1016/j.microc.2024.109967
27. Dube, A., Malode, S. J., Alodhayb, A. N., Mondal, K., & Shetti, N. P. (2025). Conducting polymer-based electrochemical sensors: Progress, challenges, and future perspectives. *Talanta open*, *11*, 100395. https://doi.org/10.1016/j.talo.2024.100395
28. Ramaraj, S. G., Alrebh, A., Elamaran, D., Zhou, H., Huang, K., Almansoori, M., ... & Tabata, H. (2025). Surface acoustic wave gas Sensors: Recent developments and their role in sensing technology. *Materials Science and Engineering: B*, *317*, 118157. https://doi.org/10.1016/j.mseb.2025.118157
29. Doll, T., Fuenzalida, V. M., Schütte, H., Gaßmann, S., Velasco-Velez, J. J., Köhler, R., ... & Viöl, W. (2024). Physical trace gas identification with the photo electron ionization spectrometer (PEIS). *Sensors*, *24*(4), 1256. https://doi.org/10.3390/s24041256
30. Mousavi, M., Akbarzadeh, V., Kazemi, M., Deng, S., & Fini, E. H. (2025). Perspective on sustainable solutions for mitigating off-gassing of volatile organic compounds in asphalt composites. *Journal of Composites Science*, *9*(7), 353. https://doi.org/10.3390/jcs9070353
31. Ministry of Environmental Protection of the People's Republic of China. (2015). Ambient air – Determination of volatile organic compounds – Collected by specially-prepared canisters and analyzed by gas chromatography/mass spectrometry (HJ 759-2015) [Standard]. China Environmental Science Press.
32. Gong, G., Zhou, B., Cao, Z., Jiang, D., & Wang, C. (2024). Enhancing accuracy and reproducibility in asphalt VOCs qualitative and quantitative analysis: Insights from laboratory studies on emission characteristics. *Construction and Building Materials*, *452*, 138997. https://doi.org/10.1016/j.conbuildmat.2024.138997
33. Moskovchenko, A., Švantner, M., & Honner, M. (2024). Detection of gunshot residue by flash-pulse and long-pulse infrared thermography. *Infrared Physics & Technology*, *140*, 105366. https://doi.org/10.1016/j.infrared.2024.105366
34. Yi, Y., Jiang, Y., Tian, T., Fan, J., Deng, C., Chen, Y., & Han, Z. (2026). A sustainable pavement coating with balanced cooling and adhesion for urban heat reduction. *Construction and Building Materials*, *507*, 145088. https://doi.org/10.1016/j.conbuildmat.2025.145088
35. Xu, Z., Han, Y., & Ren, D. (2023). Coupling Phenomenon Between Fugitive Dust and High-Temperature Tail Gas: A Thermal Infrared Signature Study. *Journal of Thermal Science and Engineering Applications*, *15*(3), 031011. https://doi.org/10.1115/1.4056406
36. Zeng, Q., Yang, S., Xu, C., Ding, J., Chen, Q., & Lu, G. (2026). Project-level automated pavement maintenance and rehabilitation decision-making with data imbalance mitigation and post-maintenance evaluation. *Automation in Construction*, *183*, 106796. https://doi.org/10.1016/j.autcon.2026.106796.